Journal of Alloys and Compounds 509 (2011) 9382–9386

Contents lists available at ScienceDirect

Journal of Alloys and Compounds

journal homepage: www.elsevier.com/locate/jallcom

Synthesis of monodispersed ultrafine Bi_2S_3 nanocrystals

Lin Shi, Dong Gu, Wei Li, Lu Han, Hao Wei, Bo Tu, Renchao Che*

Department of Chemistry, Shanghai Key Laboratory of Molecular Catalysis and Innovative Materials and Advanced Materials Laboratory, Department of Material Science, Fudan University, Shanghai 200433, PR China

ARTICLE INFO

Article history:
Received 13 June 2011
Received in revised form 14 July 2011
Accepted 15 July 2011
Available online 22 July 2011

Keywords:
Bi_2S_3 nanocrystals
Transmission electron microscopy
Monodispersed

ABSTRACT

Monodispersed ultrafine Bi_2S_3 nanocrystals of ~3 nm were synthesized via a facile and mild method, in which thioacetamide and bismuth oleate complex were used as the sulfur and bismuth precursors, respectively. The obtained Bi_2S_3 nanocrystals possessed a high surface area of 305 $m^2\ g^{-1}$. The nanostructures of Bi_2S_3 nanocrystals were characterized by X-ray diffraction (XRD), high-resolution transmission electron microscopy (HRTEM) and selective area electron diffraction (SAED) techniques. The optical property of the Bi_2S_3 nanocrystals was studied by photoluminescence spectroscopy. A remarkable blue shift and a band gap of ~1.5 eV were observed. The shape of the Bi_2S_3 nanocrystals could be tuned by adjusting the initial Bi/S molar ratio and reaction temperature, respectively. A possible burst nucleation mechanism for this monodispersed ultrafine Bi_2S_3 nanocrystals was proposed.

1. Introduction

The synthesis of semiconductor nanocrystals with controllable shape and size has been intensively pursued, which is of extreme importance for both fundamental research and technical applications [1–9]. Bi_2S_3 is a photoconducting semiconductor with a direct band gap of ~1.3 eV [10], which gives promising applications such as thermoelectricity [11], infrared spectroscopy [12], X-ray computed tomography [13], photovoltaics [14], nonlinear absorption [15] and biomolecule detection [16]. It is well known that smaller Bi_2S_3 nanocrystals possess larger specific surface area and therefore have higher photocatalytic activities on the photodegradation of rhodamine [17] and better performance in the electrochemical hydrogen storage [18].

Significant advances have been achieved in the preparation of Bi_2S_3 nanostructures with different shapes, such as nanorods [17–22], nanowires [23–26] and nanoflowers [27–29]. It is well known that one-dimensional nanorods are predominantly formed because the [0 0 1] zone axis of Bi_2S_3 crystal is its preferential growth direction [30]. Hence, it is difficult to obtain Bi_2S_3 quantum dots. Up to date, many synthetic strategies have been developed to achieve metal sulfide nanocrystals with tunable shape and size, such as homogeneous phase precipitation [31,32], reverse micelles method [33–35], thermolysis of organometallic precursors [36,37,43,44], hydrothermal or solvothermal synthesis [38], and water/toluene two-phase system reaction [39–41]. Organometallic precursors and capping reagents were reported to be used to effectively control the Bi_2S_3 nanostructures [19,20,30]. Notably, Malakooti and co-workers synthesized Bi_2S_3 nanocrystals with around 10 nm size under a heterogeneous reaction environment by using oleylamine as a surfactant and reduction agent [42]. Meanwhile, ultrathin necklace-like Bi_2S_3 nanowires were fabricated by using bismuth citrate as the bismuth precursor under a relatively low temperature [23]. However, the synthesis of monodispersed Bi_2S_3 nanocrystals with size less than 5 nm has not been reported so far.

Herein, we developed a facile and mild approach to synthesize the monodispered ultrafine Bi_2S_3 nanocrystals by using thioacetamide as a sulfur precursor. The bismuth oleate complex was obtained through the reaction between bismuth oxide and oleic acid, which was used as a bismuth precursor. Bi_2S_3 nanocrystals were formed at the interface between 1-octadecene and water phase. The monodispered Bi_2S_3 nanocrystals of about 3 nm could be obtained. The shape of the Bi_2S_3 nanocrystals could be tuned by adjusting the initial Bi/S molar ratio and reaction temperature, respectively. We have proposed a possible burst nucleation mechanism for the formation of the monodispersed ultrafine Bi_2S_3 nanocrystals.

2. Experimental procedures

2.1. Materials

Bismuth oxide, glacial acetic acid, ethanol, thioacetamide, ethyl acetate, and toluene were purchased from Shanghai Chemical Corp. 1-Octadecene (ODE) and oleic acid was purchased from Aldrich and Alfa Asear, respectively. All chemicals were used without further purification.

2.2. Synthesis of bismuth oleate complex

1.0 mmol of Bi_2O_3 and 2.0 ml of glacial acetic acid were loaded in a three-necked flask with 25 ml volume, and heated up to 140 °C with one neck open. The above mixture was stirred at 140 °C until a dry powder was formed. The powder was cooled

* Corresponding author.
E-mail address: rcche@fudan.edu.cn (R. Che).

0925-8388/$ – see front matter © 2011 Elsevier B.V. All rights reserved.
doi:10.1016/j.jallcom.2011.07.049

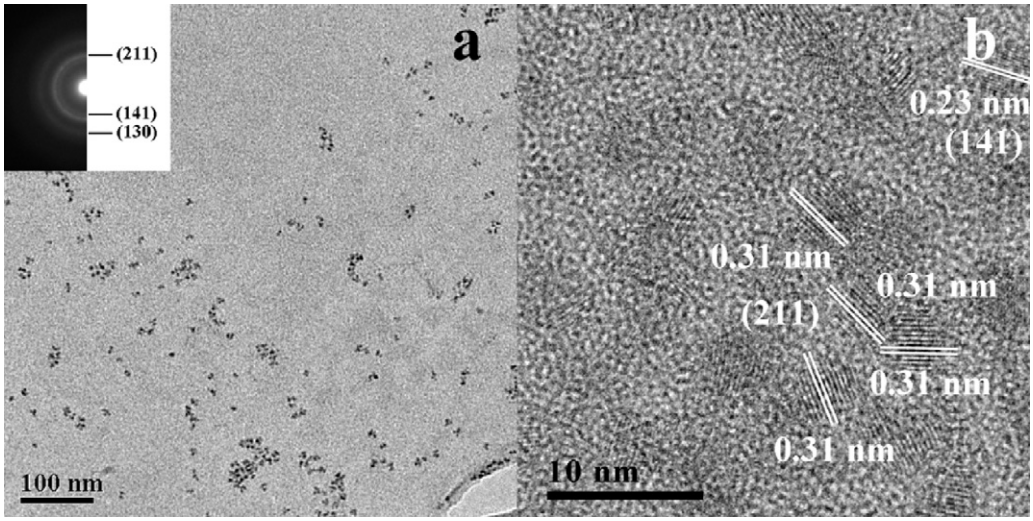

Fig. 1. (a) Typical TEM image, (inset of a) the SAED pattern, and (b) the corresponding HRTEM image of the Bi_2S_3 nanocrystals prepared at 80 °C for 10 min with the initial Bi/S molar ratio of 1/2.

down to 130 °C. Then, 10 mmol of oleic acid was added. The solution was stirred at 130 °C under an inert gas flow for 6 h. The obtained bismuth oleate complex with excess oleic acid was cooled down and diluted by adding 50 ml of ODE to form the bismuth oleate complex precursor solution.

2.3. Synthesis of Bi_2S_3 nanocrystals

2.5 ml of bismuth oleate precursor solution, 6.5 ml of ODE and 1.0 ml of oleic acid were loaded together into a 250 ml three-necked flask. The solution was stirred at 80 °C until a transparent solution was formed. Subsequently, 0.5 ml of thioacetamide aqueous solution (0.4 M) was added. The reactant solution changed to be reddish brown gradually (the color did not change to dark even after stirring for 1 day). After 10 min of reaction, 20 ml of ethyl acetate was added into the solution. The mixture was centrifuged at 10,000 rpm for 30 min. The resulted dark precipitate was washed by ethyl acetate for 3 times and dried at 50 °C for 1 day.

2.4. Characterization

X-ray diffraction patterns were recorded with a Bruker D8 X-ray diffractometer with Ni-filtered Cu Kα radiation (40 kV, 40 mA). The Raman spectra were measured at room temperature with a Renishaw invar Reflex Raman spectrometer. TEM analysis was carried out on a JEM JEOL-2100F microscope equipped with a post-column Gatan imaging filter system (GIF-Tridium) operated at 200 kV. For the TEM measurements, the Bi_2S_3 nanocrystals were dispersed in toluene, dipped and dried on a copper grid covered with a holey carbon film. Nitrogen sorption isotherms were measured at 77 K with a Micromeritics Tristar 3000 analyzer (USA). By two experimental run, 50 mg of powder samples can be prepared, which was enough for the BET measurement. Before measurement, the sample was degassed at 120 °C for 12 h. The Brunauer–Emmett–Teller (BET) method was utilized to calculate the specific surface area. The pore size distribution was derived from the adsorption branch by using the Barrett–Joyner–Halenda (BJH) model. The photoluminescence (PL) spectra were recorded on a Hitachi F-4500 fluorescence spectrophotometer with an excitation wavelength of 750 nm.

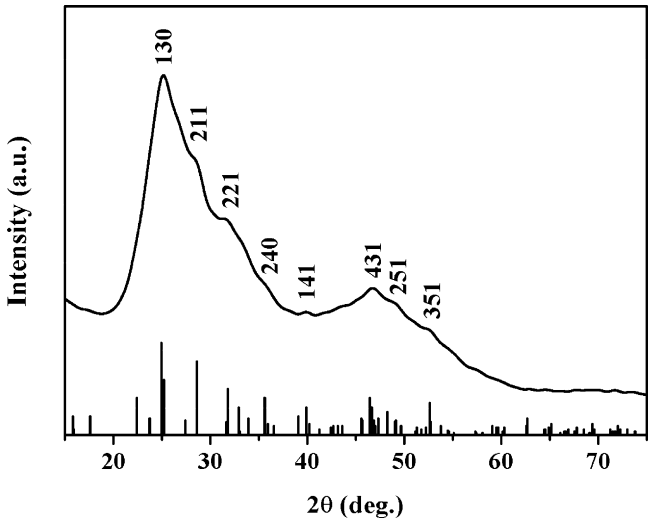

Fig. 2. Wide-angle XRD pattern of Bi_2S_3 nanocrystals prepared at 80 °C for 10 min with the initial Bi/S molar ratio of 1/2. The standard Bi_2S_3 diffraction lines (JCPDS: 17-320) are shown as vertical bars.

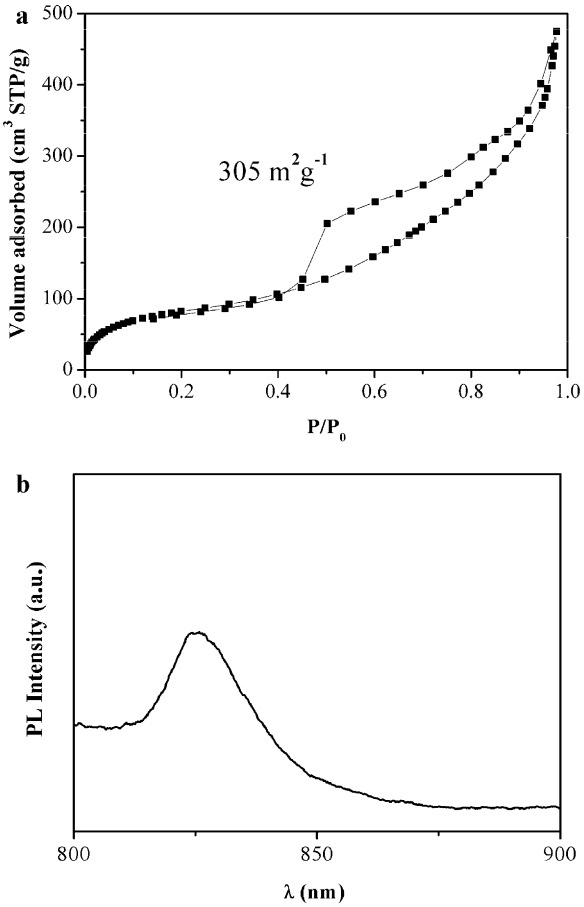

Fig. 3. (a) Nitrogen sorption isotherms and (b) PL spectrum of Bi_2S_3 nanocrystals prepared at 80 °C for 10 min with the initial Bi/S molar ratio of 1/2.

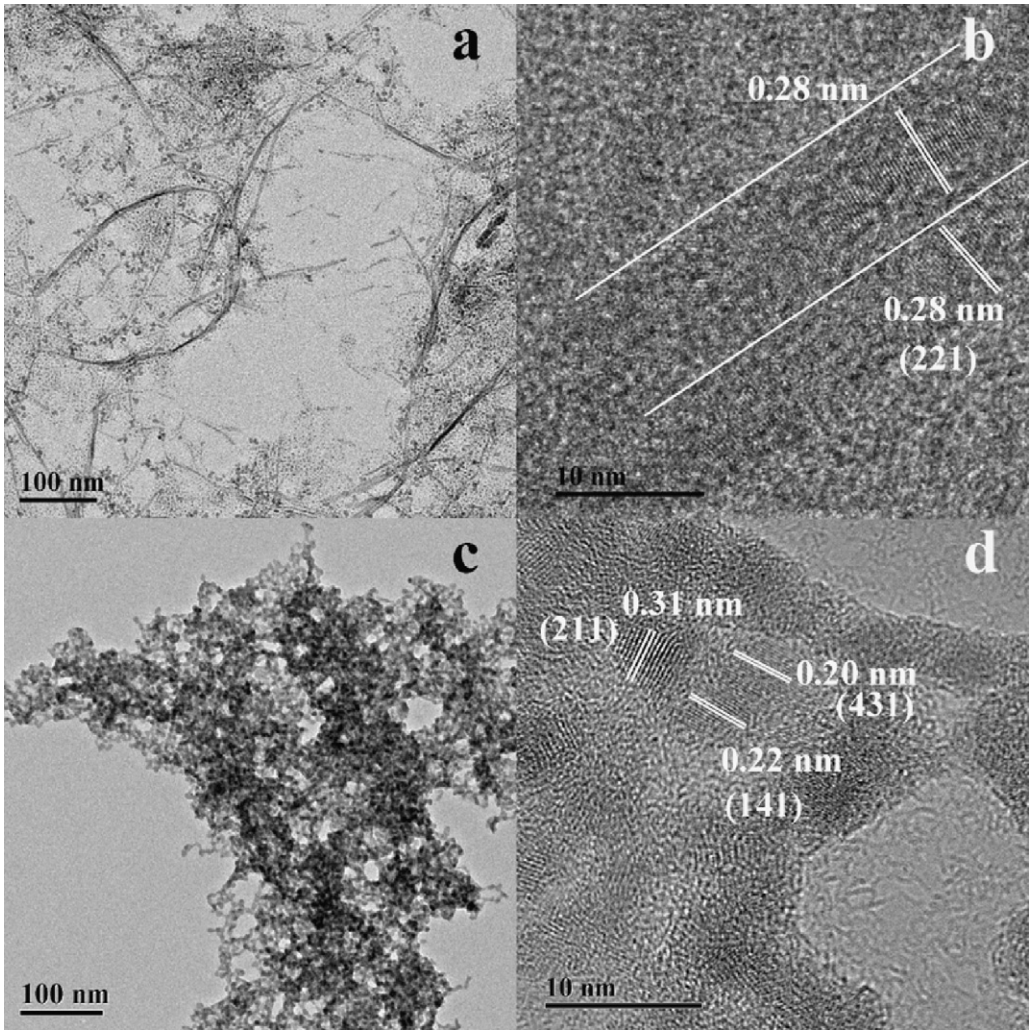

Fig. 4. TEM and HR-TEM images of Bi_2S_3 nanocrystals prepared at 80 °C for 10 min with the initial Bi/S molar ratio of (a and b) 2/3 and (c and d) 1/4.

3. Results and discussion

TEM image of the Bi_2S_3 nanocrystals (Fig. 1a) show the uniform spherical morphology of ~3 nm, which were prepared at 80 °C for 10 min with the initial molar ratio Bi/S of 1/2. The SAED (inset of Fig. 1a) displays a multi-ring diffraction feature, which can be attributed to the nature of monodispersed ultrafine Bi_2S_3 nanocrystals. Three main atomic lattice fringes are observed, which including (2 1 1), (1 4 1) and (1 3 0) crystal faces, indicating the high crystallization degree of the obtained samples. It can be seen that the size distribution of the as-synthesized Bi_2S_3 nanoparticles is quite sharp. HRTEM image clearly reveals the well-defined single-crystal structure of the Bi_2S_3 nanoparticles (Fig. 1b). The fringes have been measured to give a *d*-spacing of about 0.31 nm, corresponding to the (2 1 1) crystal plane of orthorhombic Bi_2S_3.

Wide-angle XRD pattern of the Bi_2S_3 nanoparticles is shown in Fig. 2. The diffraction peaks could be well indexed to the orthorhombic phase of Bi_2S_3 (JCPDS: 17-320). The XRD peaks are relatively broad, further confirming the ultrafine size of the nanoparticles. The energy-dispersive spectroscopy (EDS) is performed to further determine the chemical composition of the nanoparticles (SI: Fig. S1). The presence of Bi and S elements with molar ratio of ~2:3 demonstrates the formation of Bi_2S_3 nanocrystals. The peaks in the Raman spectra further indicate the formation of the Bi_2S_3 nanocrystals (SI: Fig. S2), which match well with the reported results [13].

The BET surface area calculated from the nitrogen adsorption isotherms (Fig. 3a) is up to as high as 305 $m^2 g^{-1}$, which may be attributed to the stacking spaces of ultrafine Bi_2S_3 nanoparticle. Fig. 3b depicts the PL spectrum of the Bi_2S_3 nanocrystals excited with a wavelength of 750 nm. The PL spectrum shows an emission peak centered at around 825 nm with an impressive full width at half-maximum (FWHM) as small as 17 nm, which could be attributed to the narrow size distribution of the Bi_2S_3 nanocrystals. The emission peak exhibited a remarkable blue shift relative to bulk Bi_2S_3 (E_g = 1.3 eV), implying that the photoconducting behavior of Bi_2S_3 nanocrystals belongs to a typical quantum-confinement effect.

To investigate the influences of the initial Bi/S molar ratio on the shape of the obtained nanocrystals, the initial Bi/S molar ratio was varied from 2/3 to 1/4, while the other experimental conditions were maintained. The reaction rate can be examined by monitoring the color change of the reaction solution. In the case of Bi/S = 2/3, it took ~15 min for the solution to change from light yellow (bismuth oleate complex precursor) to reddish brown (Bi_2S_3 nanocrystals) (SI: Fig. S3). When the Bi/S ratio is 1/2, it took ~5 min for the solution to change to be reddish brown color. When the Bi/S is 1/4, the solution color immediately turned reddish brown and became dark black (bulk Bi_2S_3) after 5 min, followed by the precipitation of

the black Bi_2S_3 solids. According to the above observations, it could be concluded that the reaction rate of thioacetamide and bismuth oleate complex increases with the increasing initial Bi/S molar ratio.

Furthermore, there are a lot of nuclei with "magic size", except a portion of nanoparticles with ~3 nm size, as shown in the TEM images of Bi_2S_3 materials obtained at 80 °C for 10 min with the initial Bi/S molar ratio of 2/3 (Fig. 4a and b), which are clusters with no more than one unit cell of the bulk crystal and close-shell structures in the size range between 1 and 2 nm [45]. Remarkably, nanofibers with diameters of about 2 nm and length of several hundred nanometers are also observed. When the initial Bi/S molar ratio is 1/4, the Bi_2S_3 nanocrystals aggregate severely, as shown in the TEM image (Fig. 4c). The HRTEM image (Fig. 4d) reveals that the size of individual Bi_2S_3 nanocrystal is still comparable to that of the typical Bi_2S_3 nanocrystals with the initial Bi/S molar ratio of 1/2, suggesting that the Bi/S ratio may have little influence on the particle size.

In the case of Bi/S = 2/3, the reaction rate (nucleation and growth) was relatively slow, as confirmed by the TEM image of Bi_2S_3 materials obtained at 80 °C for 5 min (SI: Fig. S4a). At the early stage, besides some nanoparticles of ~3 nm, the "magic size" nuclei were found. These "magic size" nuclei could assemble together and form nano-necklaces to decrease the surface free energy of the reaction system [46]. There are no more sulfur sources to supply the "magic size" nuclei to grow and form larger nanoparticles. Therefore, the nuclei would assemble and form nanofibers with prolonging the reaction time of 10 min (Fig. 4a and b). While in the case of Bi/S = 1/2, most of the Bi_2S_3 nanocrystals would grow and form large nanoparticles (~3 nm in size) (SI: Fig. S4b). When the Bi/S was 1/4, the Bi_2S_3 nanocrystals would grow large (~3 nm in size) and aggregate easily (Fig. 4c and d). Thus the initial Bi/S molar ratio could affect the morphology of final Bi_2S_3 products.

The effect of the sulfur precursor of thioacetamide on the Bi_2S_3 products is also studied [47]. In the water/toluene two-phase system, thiourea was generally used as the sulfur precursor to slow down the nucleation and growth rate [38–40]. Both the nucleation and growth stages are expected to be quite long as the releasing rate of H_2S gas from thiourea is low. When thiourea was used as the sulfur precursor, no Bi_2S_3 product was obtained at 80 °C after reaction for 24 h. In contrast thioacetamide is unstable and easily decompose to release H_2S even at room temperature. In the case of our experiment with thioacetamide as the sulfur precursor, most of the Bi_2S_3 nanocrystals were formed at the beginning of 5 min (SI: Fig. S4b), indicating that the nucleation period was short and the growth rate was fast. Since only 0.5 ml of thioacetamide aqueous solution was introduced into 10 ml of ODE solution under vigorous stirring, the released H_2S gas from thioacetamide could immediately migrate and reach the interface between ODE and water. The size of the Bi_2S_3 nanoparticles would not change obviously even after 2 h (SI: Fig. S4c and d). Therefore, the whole process can be divided into two stages. At the early stage, a fast growth takes place after a burst of nucleation which is completed within a rather short time (several minutes). At the latter stage, the growth process is extremely slow and extends to a long time (up to several days). A higher temperature can accelerate the latter stage, which could be proved by the TEM images of products obtained when the reaction temperature and time were increased to be 90 °C and 30 min, respectively (SI: Fig. S5). Interestingly, some by-product of nanorods of ~3 nm in diameter and ~12 nm in length were formed.

According to the above results, we propose a burst nucleation mechanism to explain the formation of the Bi_2S_3 nanocrystals. As shown in Fig. 5, the quickly released H_2S gas from thioacetamide could reach the interface of the two solutions of water and toluene immediately. The H_2S reacts with the bismuth oleate complex to trigger the formation of a large amount of Bi_2S_3 nuclei. The OA-capped nuclei are hydrophobic and re-diffused into the ODE solution after the nuclei grow and form larger Bi_2S_3 nanocrystals. The growth of nanocrystals slow down and stops as the excess H_2S gas escapes from the interface of water and toluene.

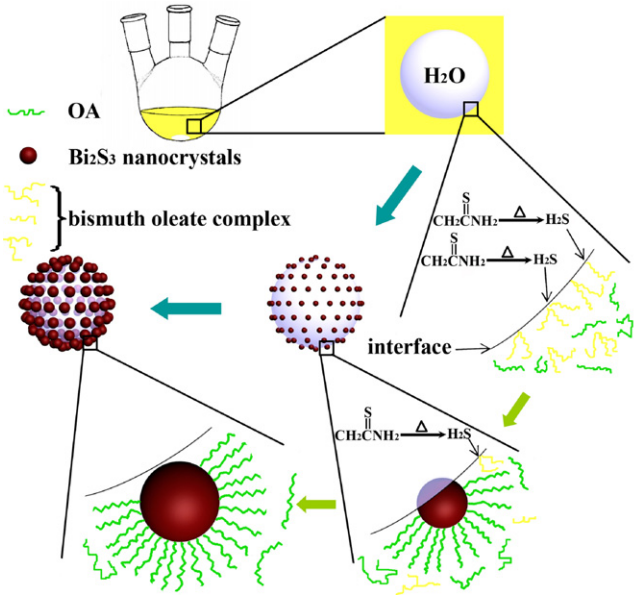

Fig. 5. The scheme of the formation mechanism of Bi_2S_3 nanocrystals.

4. Conclusions

Highly crystalline and monodispered Bi_2S_3 nanocrystals of about 3 nm have been synthesized via a facile and mild method for the first time. The as-prepared nanocrystals show a high BET surface area of 305 $m^2 g^{-1}$. The Bi_2S_3 nanocrystals exhibit PL emission peaked at 825 nm. The band gap is measured to be 1.5 eV, showing a remarkable blue shift relative to bulk Bi_2S_3 due to the quantum size effects. The initial molar ratio of Bi/S and sulfur precursor could affect the formation of Bi_2S_3 nanocrystals. A possible burst nucleation mechanism has been demonstrated for the formation of the monodispersed ultrafine Bi_2S_3 nanocrystals. Our findings may provide new insight for the convenient synthesis of other ultrafine metal sulfide nanocrystals.

Acknowledgements

All authors appreciate the instructions from Prof. Dongyuan Zhao. This work is supported by the NSF of China (nos. 50872145, 20721063, 10776037, and 20821140537) and the Ministry of Science and Technology of China (973 Project no. 2007CB936301, 2009AA033701 and 2009CB930803), the State Key Basic Research Program of the PRC (2006CB932302), Shanghai Leading Academic Discipline Project (B108), and Fudan Graduate Innovation Funds. The authors are grateful to the "Shu Guang" project supported by Shanghai Municipal Education Commission and Shanghai Education Development Foundation (09SG01) and Project: 9140C4403090902.

Appendix A. Supplementary data

Supplementary data associated with this article can be found, in the online version, at doi:10.1016/j.jallcom.2011.07.049.

References

[1] A.P. Alivisatos, Nat. Biotechnol. 22 (2004) 47–52.

[2] P.O. Anikeeva, J.E. Halpert, M.G. Bawendi, V. Bulovic, Nano Lett. 9 (2009) 2532–2536.
[3] H. Lu, O. Schops, U. Woggon, C.M. Niemeyer, J. Am. Chem. Soc. 130 (2008) 4815–4827.
[4] H. Mattoussi, L.H. Radzilowski, B.O. Dabbousi, E.L. Thomas, M.G. Bawendi, M.F. Rubner, J. Appl. Phys. 83 (1998) 7965–7974.
[5] W.C.W. Chan, S.M. Nie, Science 281 (1998) 2016–2018.
[6] M. Bruchez, M. Moronne, P. Gin, S. Weiss, A.P. Alivisatos, Science 281 (1998) 2013–2016.
[7] M.C. Schlamp, X.G. Peng, A.P. Alivisatos, J. Appl. Phys. 82 (1997) 5837–5842.
[8] A.P. Alivisatos, Science 271 (1996) 933–937.
[9] S. Baskoutas, A.F. Terzis, J. Appl. Phys. 99 (2006), 013708.
[10] J. Grigas, E. Talik, V. Lazauskas, Phys. Stat. Sol. B 232 (2002) 220–230.
[11] B.X. Chen, C. Uher, L. Iordanidis, M.G. Kanatzidis, Chem. Mater. 9 (1997) 1655–1658.
[12] D. Arivuoli, F.D. Gnanam, P. Ramasamy, J. Mater. Sci. Lett. 7 (1988) 711–713.
[13] O. Rabin, J. Manuel Perez, J. Grimm, G. Wojtkiewicz, R. Weissleder, Nat. Mater. 5 (2006) 118–122.
[14] R. Suarez, P.K. Nair, P.V. Kamat, Langmuir 14 (1998) 3236–3241.
[15] X.Y. Yang, W.D. Xiang, H.J. Zhao, H.T. Liu, X.Y. Zhang, X.J. Liang, J. Alloys Compd. 509 (2011) 7283–7289.
[16] L. Cademartiri, F. Scotognella, P.G. O'Brien, B.V. Lotsch, J. Thomson, S. Petrov, N.P. Kherani, G.A. Ozin, Nano Lett. 9 (2009) 1482–1486.
[17] T. Wu, X.G. Zhou, H. Zhang, X.H. Zhong, Nano Res. 3 (2010) 379–386.
[18] L.S. Li, N.J. Sun, Y.Y. Huang, Y. Qin, N. Zhao, J.N. Gao, M.X. Li, H.H. Zhou, L.M. Qi, Adv. Funct. Mater. 18 (2008) 1194–1201.
[19] M.B. Sigman, B.A. Korgel, Chem. Mater. 17 (2005) 1655–1660.
[20] W.J. Lou, M. Chen, X.B. Wang, W.M. Liu, Chem. Mater. 19 (2007) 872–878.
[21] G. Xie, Z.P. Qiao, M.H. Zeng, X.M. Chen, S.L. Gao, Crys. Growth Des. 4 (2004) 513–516.
[22] J.L. Wu, F. Qin, G. Cheng, H. Li, J.H. Zhang, Y.P. Xie, H.J. Yang, Z. Lu, X.L. Yu, R. Chen, J. Alloys Compd. 509 (2011) 2116–2126.
[23] L. Cademartiri, R. Malakooti, P.G. O'Brien, A. Migliori, S. Petrov, N.P. Kherani, G.A. Ozin, Angew. Chem. Int. Edit. 47 (2008) 3814–3817.
[24] X.Z. Liu, J.H. Cui, L.P. Zhang, W.C. Yu, F. Guo, Y.T. Qian, Nanotechnology 16 (2005) 1771–1775.
[25] H. Zhang, Y.J. Ji, X.Y. Ma, J. Xu, D.R. Yang, Nanotechnology 14 (2003) 974–977.
[26] Y.W. Koh, C.S. Lai, A.Y. Du, E.R.T. Tiekink, K.P. Loh, Chem. Mater. 15 (2003) 4544–4554.
[27] B. Zhang, X.C. Ye, W.Y. Hou, Y. Zhao, Y. Xie, J. Phys. Chem. B 110 (2006) 8978–8985.
[28] C.J. Tang, G.Z. Wang, H.Q. Wang, Y.X. Zhang, G.H. Li, J. Nanosci. Nanotechnol. 10 (2010) 5451–5455.
[29] T. Thongtem, C. Pilapong, J. Kavinchan, A. Phuruangrat, S. Thongtem, J. Alloys Compd. 500 (2010) 195–199.
[30] J. Tang, A.P. Alivisatos, Nano Lett. 6 (2006) 2701–2706.
[31] A. Chemseddine, H. Weller, Phys. Chem. 97 (1993) 636–637.
[32] T. Vossmeyer, L. Katsikas, M. Giersig, I.G. Popovic, K. Diesner, A. Chemseddine, A. Eychmuller, H. Weller, J. Phys. Chem. 98 (1994) 7665–7673.
[33] C. Petit, M.P. Pileni, J. Phys. Chem. 92 (1988) 2282–2286.
[34] N. Herron, Y. Wang, H. Eckert, J. Am. Chem. Soc. 112 (1990) 1322–1326.
[35] R.B. Khomane, A. Manna, A.B. Mandale, B.D. Kulkarni, Langmuir 18 (2002) 8237–8240.
[36] C.B. Murray, D.J. Norris, M.G. Bawendi, J. Am. Chem. Soc. 115 (1993) 8706–8715.
[37] J. Lee, V.C. Sundar, J.R. Heine, M.G. Bawendi, K.F. Jensen, Adv. Mater. 12 (2000) 1102.
[38] X.H. Chen, L. Gao, X. Zhang, L. Gao, C. Zhang, P.Y. Kong, H. Liu, X.G. Peng, A.H. Sun, D.G. Qi, Y. Gong, Q.Y. Wang, Blood Cell Mol. Dis. 43 (2009) 98–104.
[39] D.C. Pan, S.C. Jiang, L.J. An, B.Z. Jiang, Adv. Mater. 16 (2004) 982.
[40] Q. Wang, D.C. Pan, S.C. Jiang, X.L. Ji, L.J. An, B.Z. Jiang, Chem. Eur. J. 11 (2005) 3843–3848.
[41] D.C. Pan, X.L. Ji, L.J. An, Y.F. Lu, Chem. Mater. 20 (2008) 3560–3566.
[42] R. Malakooti, L. Cademartiri, Y. Akcakir, S. Petrov, A. Migliori, G.A. Ozin, Adv. Mater. 18 (2006) 2189.
[43] R.R. Ahire, B.R. Sankapal, C.D. Lokhande, Mater. Res. Bull. 36 (2001) 199–210.
[44] V.V. Killedar, C.D. Lokhande, C.H. Bhosale, Thin Solid Films 289 (1996) 14–16.
[45] Z.A. Peng, X.G. Peng, J. Am. Chem. Soc. 124 (2002) 3343–3353.
[46] A. Narayanaswamy, H.F. Xu, N. Pradhan, M. Kim, X.G. Peng, J. Am. Chem. Soc. 128 (2006) 10310–10319.
[47] Q. Lu, F. Gao, S. Komarneni, J. Am. Chem. Soc. 126 (2004) 54–55.